Short wavelength turbulence generated by shear in the QH-mode edge on DIII–D

Citation: Rost, J. C., M. Porkolab, J. Dorris, and K. H. Burrell. "Short Wavelength Turbulence Generated by Shear in the Quiescent H-Mode Edge on DIII–D." Phys. Plasmas 21, no. 6 (June 2014): 062306.

As Published: http://dx.doi.org/10.1063/1.4883135

Publisher: American Institute of Physics (AIP)

Persistent URL: http://hdl.handle.net/1721.1/98285

Version: Author's final manuscript: final author's manuscript post peer review, without publisher's formatting or copy editing

PSFC/JA-14-14

Short wavelength turbulence generated by shear in the QH-mode edge on DIII–D

J.C. Rost, M. Porkolab, J. Dorris, and K.H. Burrell*

June 2014

Plasma Science and Fusion Center
Massachusetts Institute of Technology
Cambridge, MA 02139 USA

*General Atomics
P.O. Box 85608
San Diego, CA 92186-5608, USA

This work was supported by the U.S. Department of Energy under DE-FG02-94ER54235 and DE-FC02-04ER54698. Reproduction, translation, publication, use and disposal, in whole or in part, by or for the United States government is permitted.

Submitted for publication to *Physics of Plasmas*.

Short wavelength turbulence generated by shear in the QH-mode edge on DIII–D

J.C. Rost,[1] M. Porkolab,[1] J. Dorris,[1] and K.H. Burrell[2]

[1)] *Plasma Science and Fusion Center, Massachusetts Institute of Technology, Cambridge, Massachusetts 02139, USA*

[2)] *General Atomics, P.O. Box 85608, San Diego, California 92186-5608, USA*

(Dated: 30 May 2014)

A region of turbulence with large radial wavenumber ($k_r\rho_s > 1$) is found in the high-shear portion of the plasma edge in Quiescent H-mode (QH-mode) on DIII–D using the Phase Contrast Imaging (PCI) diagnostic. At its peak outside the minimum of the E_r well, the turbulence exhibits large amplitude $\tilde{n}/n \sim 40\%$, with large radial wavenumber $|\bar{k}_r/\bar{k}_\theta| \sim 11$ and short radial correlation length $L_r/\rho_i \sim 0.2$. The turbulence inside the E_r well minimum is characterized by the opposite sign in radial wavenumber from that of turbulence outside the minimum, consistent with the expected effects of velocity shear. The PCI diagnostic provides a line-integrated measurement of density fluctuations, so data is taken during a scan of plasma position at constant parameters to allow the PCI to sample a range in k_r/k_θ. Analysis of the Doppler Shift and plasma geometry allows the turbulence to be localized to a narrow region 3 mm inside the last closed flux surface (LCFS), outside the minimum of the E_r well. The turbulence amplitude and radial wavenumber and correlation length are determined by fitting the PCI results with a simple non-isotropic turbulence model with two regions of turbulence. These PCI observations, made in QH-mode, are qualitatively similar to those made in standard ELM-free H-mode and between edge localized modes (ELMs), suggesting a similar role for large k_r turbulence there.

PACS numbers: 52.35.Ra,52.55.Fa,52.70.Kz,52.25.Gj

I. INTRODUCTION

The search for reactor-compatible high-performance plasmas has led to the discovery of multiple varieties of steady-state ELM-free regimes with energy confinement similar to that of H-mode yet without significant impurity accumulation. One such regime that has received extensive study at DIII–D[1] is the quiescent H-mode (QH-mode), which exhibits constant plasma density and impurity levels and no ELMs with a strong energy transport barrier in the edge.[2] A large coherent electromagnetic fluctuation is seen inside the separatrix and is referred to as the edge harmonic oscillation (EHO) because the non-sinusoidal perturbation appears as a series of harmonics in a power spectrum.[3] QH-mode was initially attained with neutral beam heating in the direction counter to the plasma current but has now been achieved with balanced and co-current neutral beam injection.[4,5] The QH-mode plasma provides a valuable platform for the study of edge turbulence and transport. Edge transport in general is much less well understood than transport in the plasma core, where large scale simulations of ion temperature gradient (ITG) and trapped trapped electron mode (TEM) turbulence have reached maturity and provide true predictive capabilities.[6] This is true despite the successes in some areas, such as establishing the thresholds that define the pedestal plasma pressure in ELMing H-mode and QH-mode.[7] Work remains to understand the role that broadband turbulence may play in establishing the threshold conditions for these regimes and in regulating the particle and heat transport individually, including interactions with other edge parameters such as plasma rotation and neutral populations.[8] The computational problem is made more difficult by the complex geometry and the short scale lengths, among other factors.

This work presents studies of broadband fluctuations in the pedestal of a QH-mode plasma in a range of wavenumbers and frequencies that is generally poorly diagnosed. The edge develops large $\mathbf{E}\times\mathbf{B}$ velocities and large velocity shear, leading to turbulence suppression[9] and also to increased Doppler shift, short radial correlation lengths, and larger radial wavenumbers.[10] The expected changes to the shape of the power spectrum may result in a significant portion of the spectral power being shifted outside the range of sensitivity of a given diagnostic due to limits in spatial resolution or frequency bandwidth, leading to measurements of turbulence amplitude which are too low. An accurate measurement of the spectral distribution and total amplitude is needed before theories of edge turbulence can be

assessed. The phase contrast imaging (PCI) diagnostic has excellent frequency bandwidth and spatial response perpendicular to the laser probe beam. Because the measurements are line integrated, additional information is required to interpret the results. For example, core turbulence measurements have been combined with gyrokinetic modeling to make the PCI measurements quantitatively meaningful.[11–13] In the experiment described here, the QH-mode plasma is shifted in space, allowing the PCI measurement to cover multiple physical locations and many separate portions of wavenumber space. Quantitative results can thereby be obtained that are unavailable from the PCI data in a stationary plasma.

In Sec. II we describe the PCI and its operation, describe the QH-mode plasma discharges in this experiment and present the general characteristics of the PCI turbulence data acquired. In Sec. III we show that the PCI data represents turbulence localized in the E_r well; this is shown using geometric effects and Doppler shift in Sec. III A and using a simple turbulence model in Sec. III B. The summary and conclusions are given in Sec. IV.

II. EXPERIMENTAL METHOD

A. Operation of PCI

Phase contrast imaging is an internal reference beam interferometry technique. Invented by Frits Zernike for microscopy, the application to tokamak plasmas was developed by H. Weisen.[14] The PCI on DIII–D has been used to study a variety of turbulence and transport phenomena including H-mode transitions,[15] zonal flows,[16] and edge localized modes.[17] The DIII–D PCI experimental setup[18,19] is typical of installations on tokamak devices. A 0.05 m diameter CO_2 laser beam at $\lambda_0 = 10.6$ μm is used to probe the plasma, passing almost vertically through the plasma where variations in plasma density distort the wavefronts. The PCI beam path at the time of these experiments is shown in Fig. 1. An optical element called a phase plate turns these phase variations into amplitude variations which are imaged onto a 16 channel HgMnTe detector. The detector bandwidth is roughly 10 MHz, higher than the typical signals of interest (< 1 MHz). The magnification of the imaging system sets the effective spatial resolution perpendicular to the beam, which in turn dictates the maximum resolvable wavenumber. The highest accessible wavenumber is ultimately limited by the aperture of the vessel windows. In practice, signal is not seen much above

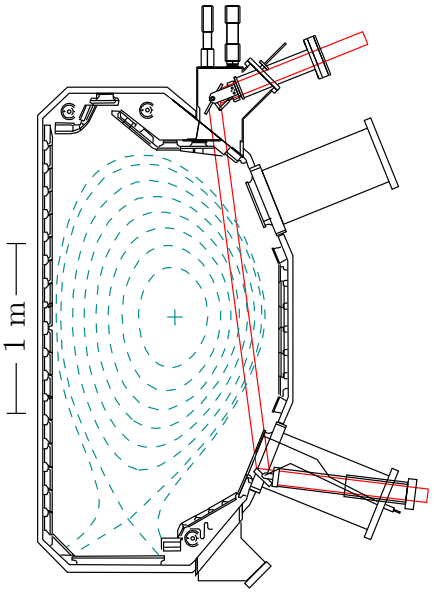

FIG. 1. PCI beam path (solid red lines) through the plasma at the time of the experiments described here. Magnetic flux surfaces are shown as dashed lines.

$k_{\mathrm{pci}} = 20$ cm^{-1}, even though the instrumental limit is higher. Detection of long wavelength modes is limited by scattering requirements, with $k_{\mathrm{min}} = 0.5$ cm^{-1} in our current setup.

The signal on detector element i is proportional to the perturbed density integrated along a chord through the plasma,

$$s_i \propto \int \tilde{n}_e(x_i, y) dy, \tag{1}$$

where x is a coordinate perpendicular to the laser beam and the y direction is along the beam. For a vertical PCI beam, Eq. (1) becomes

$$s_i \propto \int \tilde{n}_e(R_i, z) dz, \tag{2}$$

where R, z are the normal cylindrical coordinates, showing that information about vertical variation is lost while information about radial variation is retained. Note that the detector channels are equally spaced. The signals are generally transformed to provide a power spectrum $S(f, k_{\mathrm{pci}})$, where k_{pci} is perpendicular to the laser beam. The precise mapping from k_{pci} to k_r, k_θ varies along the beam and depends on the plasma geometry.

A rotating filter based on scattering angle relative to the magnetic field provides some localization along the beam.[19] The localization is optimal for wavenumbers higher than those studied here as well as lower q_{95}, but contributions from edge-localized turbulence at lower

wavenumbers can be separated into components from above and below the midplane. The instrumental response is broad for such wavenumbers, so there is a central filter position which responds to electrostatic turbulence along the entire beam path. In this experiment, the filter was swept every 0.2 s.

B. QH-mode experiment

A QH-mode plasma obtained with 6 MW of counter-current neutral beam heating power was reproduced six times. The PCI data used in this work is a combination of data from all six shots. The high reproducibility of QH-mode plasmas makes them uniquely suited to this investigation. The plasma parameters were constant throughout the QH-mode phase with line-averaged density $\bar{n}_e = 2 \times 10^{19}$ m^{-3} and central ion temperature $T_{i0} = 11$ keV, with multiple seconds entirely free of ELMs, as shown in Fig. 2. The outer gap, between the plasma and the outboard limiter, is scanned by 0.13 m while maintaining constant plasma parameters, allowing diagnostics to take measurements at finely spaced radial locations. The local plasma parameters in the edge also remain constant, as demonstrated in Fig. 3 by plots of q from the magnetic reconstruction, n_e from Thomson scattering,[20] and T_i from charge exchange recombination (CER) spectroscopy.[21] The CER diagnostic also provides the measurements that allow the determination of the radial electric field E_r and hence the **E**×**B** velocity perpendicular to the magnetic field. During H-mode, an E_r well develops in the plasma edge, and the corresponding **E**×**B** velocity is shown in Fig. 3 for the shots under study here. The **E**×**B** velocity is relatively large in amplitude, and there exists a strong gradient in velocity which can be expected to shear structures in plasma turbulence such as eddies. The consistency of edge parameters during a plasma position sweep has been used previously to increase the effective resolution of the edge E_r measurement in QH-mode.[22]

C. PCI results

An example of a PCI power spectrum $S(f)$ recorded during the outer gap sweep is shown in Fig. 4. The series of harmonics from the EHO is seen below 100 kHz along with broadband turbulence with frequencies up to 500 kHz.

Figure 5 shows a comparison of PCI 2d spectra $S(k_{\rm pci}, f)$ for three different plasma

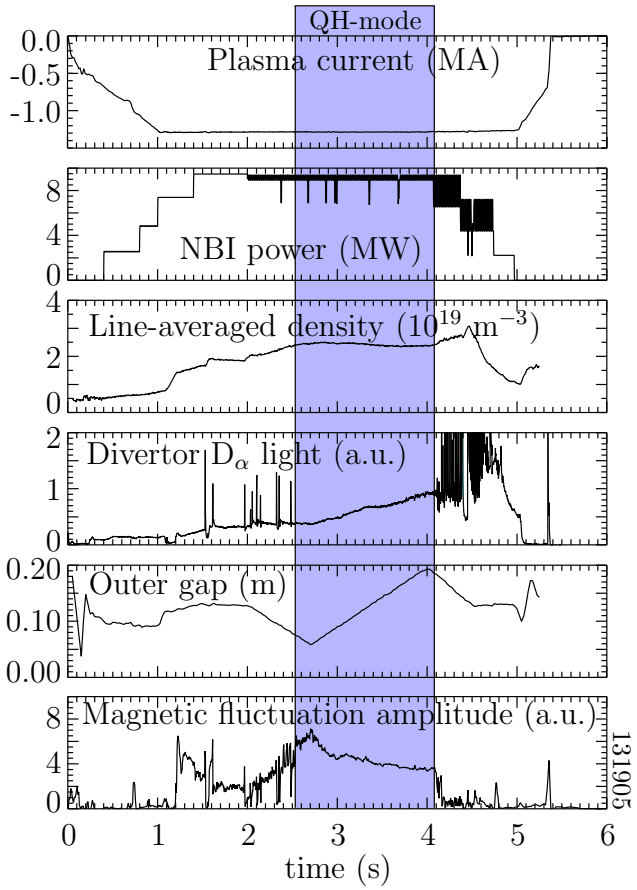

FIG. 2. The QH-mode phase (shaded region) exhibits constant density with no ELMs seen on the D_α signal. The presence of the EHO is reflected in the magnetic fluctuations. An outer gap scan is performed between 2.0 and 4.5 s.

locations in QH-mode, as well as one L-mode spectrum. The L-mode spectrum is roughly symmetric in the sign of $k_{\rm pci}$, and the turbulence is maximum at the lowest frequency. In constrast, the H-mode spectra are strongly asymmetric in $k_{\rm pci}$, and the signal exhibits high-frequency peaks at well-defined phase velocity $v = 2\pi f/k_{\rm pci}$ (which is not a plasma velocity, as discussed below). Several features change with relative position between the beam and the plasma edge, most importantly the asymmetry in $k_{\rm pci}$ and the phase velocity. Note also that the phase velocity is different for positive and negative $k_{\rm pci}$, and turbulence below 100 kHz exhibits a much lower phase velocity. The analysis below will focus on the turbulence above 100 kHz, because this is well-separated from the EHO and the large phase velocity suggests a relation to the plasma edge.

The spatial localization achievable at the dominant wavenumber seen in Fig. 5 is only

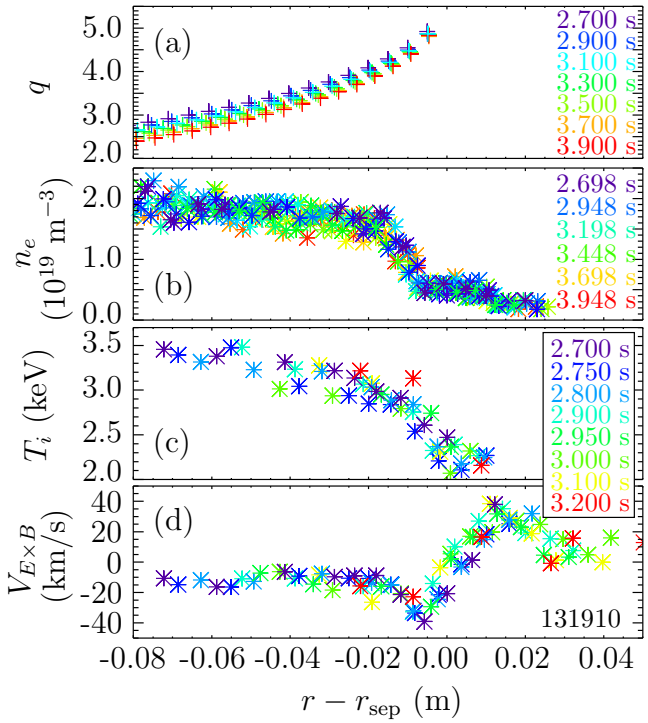

FIG. 3. The edge parameters remain nearly constant during the edge position scan, as shown by (a) the safety factor q from the magnetic reconstruction, (b) the electron density from Thomson scattering, and (c) the ion temperature and (d) the **E**×**B** velocity in the plasma edge as measured via charge exchange recombination spectroscopy. Measurements at different times during the position scan are plotted relative to the separatrix location at the time the data is acquired, indicating that parameters remain constant with respect to the separatrix.

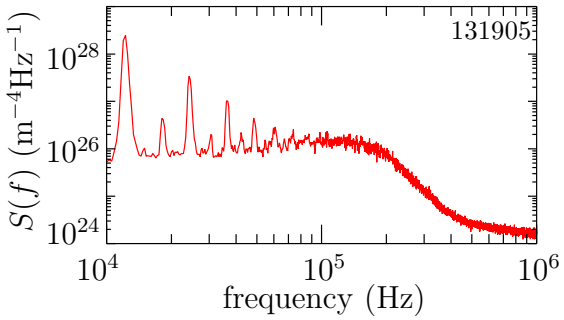

FIG. 4. PCI power spectrum $S(f)$ shows the EHO at multiples of 12 kHz with weaker harmonics of 6 kHz and broadband turbulence above the noise floor up to 500 kHz.

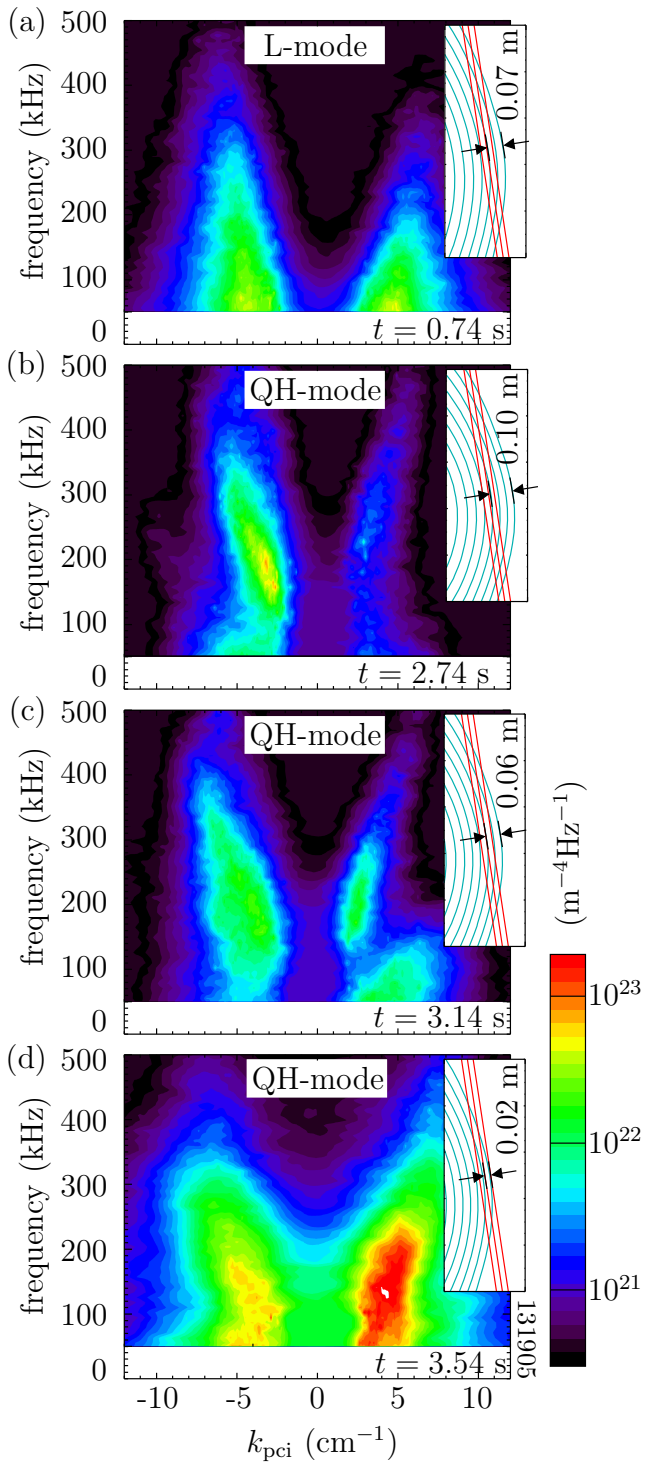

FIG. 5. PCI 2d spectrum $S(k_{\mathrm{pci}}, f)$ in L-mode (a) contrasts with spectra in QH-mode taken at three different plasma positions (b)–(d) reaching up to 0.105 m inside the separatrix. Spectra from different relative beam positions show different apparent phase velocities $2\pi f/k_{\mathrm{pci}}$ and different relative amplitudes between the $k < 0$ and $k > 0$ components.

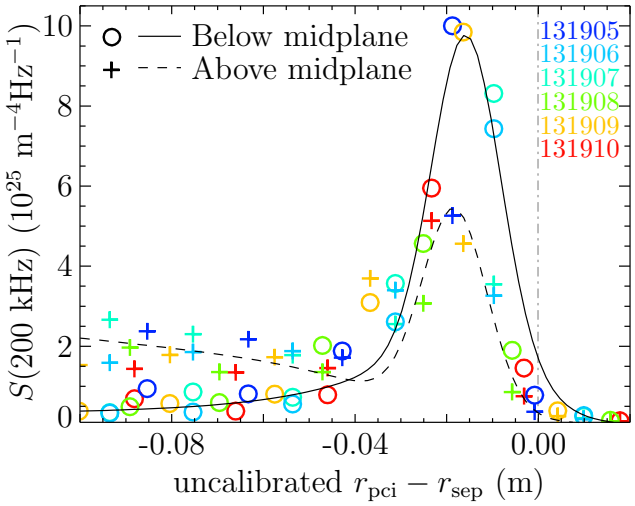

FIG. 6. Amplitude of the PCI signal measured during a scan of plasma position. Dependent axis is the minimum radius of the PCI laser beam with respect to the separatrix. Vertical dash-dot line indicates the plasma edge position such that the center of the PCI beam is tangent to the separatrix. PCI beam position is determined ±15 mm. Contributions from above and below the midplane are plotted separately. A large peak occurs when the center of the PCI beam is tangent to a flux surface about 16 mm inside the separatrix, indicating that turbulence in the parameter range measured is largest there.

sufficient to differentiate between signal sources above and below the midplane. Turbulence is seen to be propagating radially inward ($k_{\mathrm{pci}} < 0$) above the midplane (toward the tokamak axis at $R = 0$) and outward ($k_{\mathrm{pci}} > 0$) below the midplane, indicating propagation in the electron drift or $k_\theta > 0$ direction. This was found to be true for all plasma regions sampled by the PCI in this experiment for all $f > 100$ kHz. At the wavenumbers of interest here, there is a large overlap in the instrumental response to signals from different plasma regions, so data for analysis was selected from time periods when the filter allowed signal from all regions of the beam path simultaneously. The strong poloidal propagation allowed the data to be split between above and below the midplane using the sign of k_{pci}, rather than the more complex process of fitting the instrumental response over a complete filter sweep.

The PCI signal is an order of magnitude larger when the beam is nearly tangent to the plasma edge as shown in Fig. 6, indicating that the turbulence seen by the PCI laser beam originates in a region near the separatrix. Note that the amplitude difference between these components includes effects of the integration length and the sampling of k_r, k_θ space, as

discussed at length in the next section.

III. INTERPRETATION OF EXPERIMENTAL RESULTS

A. Turbulence radial location and Doppler shift

At a given frequency, the power spectra $S(k_{\rm pci}, f = f_0)$ is observed to have a narrow peak and therefore a well-defined dominant $k_{\rm pci}$. The H-mode spectra in Fig. 5b-c show that frequency is approximately proportional to the dominant $k_{\rm pci}$, indicating that the signal is dominated by turbulence with the same **E**×**B** velocity and hence is localized radially. In contrast, the L-mode signal in Fig. 5a is consistent with turbulence with a range of Doppler shifts and therefore is not localized. Assuming the turbulence is radially localized at $r_{\rm t}$, the value of k_θ can be determined from $k_{\rm pci}$, $r_{\rm t}$, and the plasma geometry. The strong Doppler shift in the edge of the QH-mode plasma results in the relation $f = Vk_\theta/2\pi$ where V is the **E**×**B** plasma velocity, which for this analysis becomes

$$f = V(r_{\rm t}) \times k_\theta(k_{\rm pci}, r_{\rm t}, R_{\rm sep})/2\pi, \tag{3}$$

where we parameterize the changing plasma edge location with $R_{\rm sep}$. We solve for the value of $r_{\rm t}$ so that Eq. (3) is valid for all $R_{\rm sep}$ as the plasma location is scanned. In other words, the observed $k_{\rm pci}$ at $f = f_0$ varies during the scan in plasma location, but the underlying k_θ does not, and the geometry of the measurement thereby allows us to determine the radial location of the turbulence. The radial location of the turbulence determined this way from the Doppler shift is $r_{\rm sep} - r_{\rm t} = 3 \pm 1$ mm, that is, the turbulence is largest 3 mm inside the separatrix. Note that this determination of the turbulence location is based on the magnetic geometry from the EFIT reconstruction and is independent of small errors in the location of the PCI beam. Thus the peak turbulence is localized with an accuracy of ±1 mm (assuming no EFIT error) while the PCI beam location is known only to ±15 mm. We can thus determine a correction to the PCI beam location, which is applied in the analysis below. If this analysis is performed for the entire range of frequencies, the frequency increases linearly in wavenumber with an offset as shown in Fig. 7, indicating that the turbulence has a finite frequency in the plasma frame.

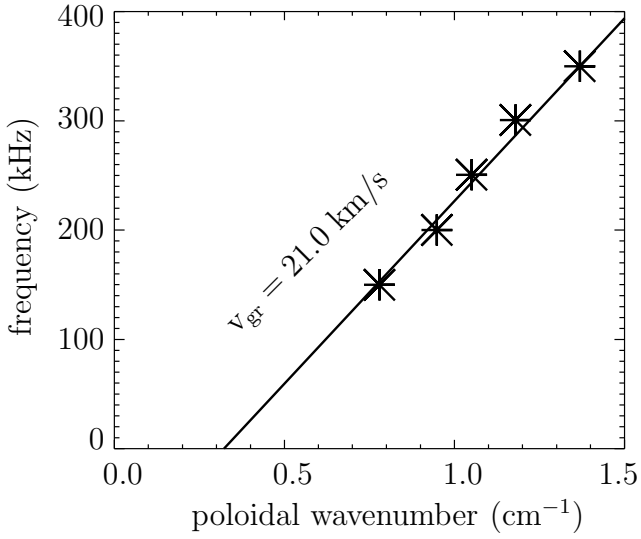

FIG. 7. Turbulence frequency plotted against the values of k_θ calculated from PCI results. Resulting group velocity is consistent with **E**×**B** velocity in E_r well.

B. Comparison with analytic model

The PCI RMS signal amplitude cannot be interpreted directly as a turbulence amplitude because the measurement is line integrated (Fig. 1 and Eq. (1)), leading to dependencies on plasma geometry, spatial extent of the turbulence, and correlation lengths. The scanning of the plasma location in this experiment however provides sufficient data to allow the determination of a complete description of the turbulence, if simplifying assumptions are made. In what follows below, a simple analytic model of the turbulence was used, and the free parameters were varied to match the experimental results.

For the purposes of the analytic model, the turbulence is assumed to be fully developed and completely characterized by a correlation function

$$C_{r\theta}(\Delta r, \Delta\xi) = e^{-(\Delta r/L_r)^2} e^{-(\Delta\xi/L_\theta)^2} \times \cos(\bar{k}_r \Delta r + \bar{k}_\theta \Delta\xi) \tag{4}$$

where the radial and poloidal correlation lengths are L_r and L_θ and $\Delta\xi$ is a poloidal distance ($\Delta\xi = r \cdot \Delta\theta$ in a circular plasma). The high shear also suggests that L_r is much shorter than L_θ, consistent with the measurements showing significant spectral power at $k_r > k_\theta$. The poloidal correlation length can then be estimated from the wavenumber spectrum $S(k_{\rm pci})$ under the assumption that $L_r \ll L_\theta$.

The expected amplitude of the PCI signal is found by combining Eq. (1) and Eq. (4)

$$\begin{aligned}\langle s(x)^2\rangle &= \iint dy_1 dy_2 \langle \tilde{n}_e(x,y_1)\tilde{n}_e(x,y_2)\rangle \\ &= \tilde{n}^2 \iint dy_1 dy_2 C_{xy}(0, y_1 - y_2)\end{aligned} \tag{5}$$

using x as a coordinate across the beam and y as a coordinate along the beam and $\tilde{n}$ representing the turbulence amplitude, $\tilde{n}^2 = \langle \tilde{n}_e^2(x,y)\rangle$. The fluctuation amplitude $\tilde{n}$ is zero outside the narrow radial region of turbulence. At each point, the x and y coordinates must be transformed into r, θ space so that the correlation function can be evaluated in the form of Eq. (4).

A simplified form of Eq. (5) can be used when the magnetic geometry is approximately Cartesian over the intersection between the PCI beam and the turbulence region,

$$\langle s(x)^2\rangle = \tilde{n}^2 \int_0^w dy (w-y) C_{xy}(0,y), \tag{6}$$

where w is the width of the turbulence along the beam path. The form in Eq. (6) is used to find approximate values for the free parameters, with the final fit performed using Eq. (5). No difference is seen except where the beam is approximately tangent to the turbulence region. The geometrically simplified form in Eq. (6) speeds up the computation by a factor of 10^6 compared to Eq. (5).

A simple analytic form

$$\langle s^2\rangle = \tilde{n}^2 w L e^{-(kL/2)^2} \tag{7}$$

is found in the limit that the path length through the turbulence is much greater than the correlation length $w \gg L$, where the correlation length L and the wavenumber k are the values properly evaluated along the beam direction.

Based on results of the previous section, we assume that the turbulence is radially localized to two thin shells with different parameters. The locations of the two shells are initially based on the E_r well in Fig. 3, because the variation in shear is believed to generate the two regions with different $\bar{k}_r$, corresponding to the inner slope and outer slope of the E_r well. Each region fills the volume between two flux surfaces, and the turbulence parameters are constant in the region, including amplitude, correlation lengths, and characteristic wavenumbers $\bar{k}_r$ and $\bar{k}_\theta$. The two regions of turbulence are assumed to be uncorrelated, so square amplitudes from each are added in calculating the expected PCI signal.

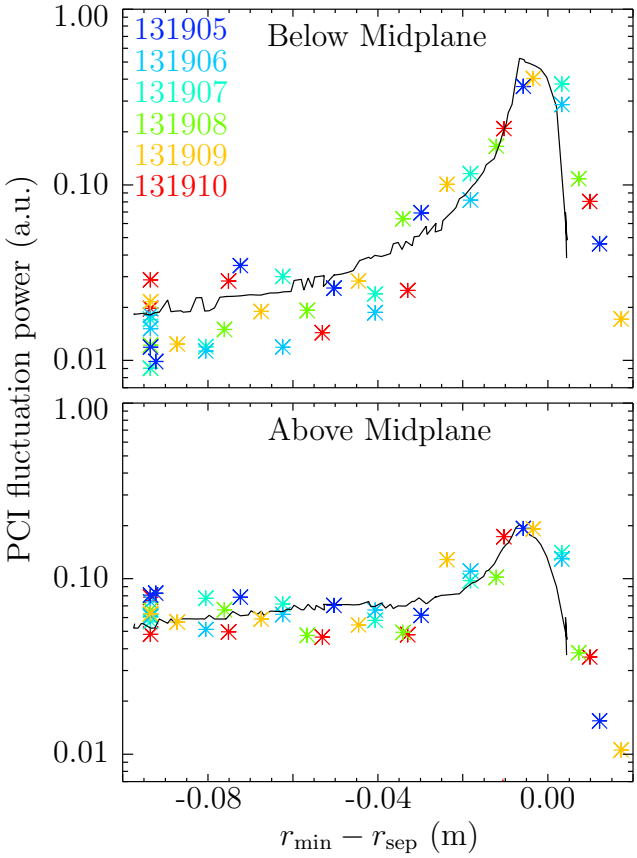

FIG. 8. Comparison of experimental PCI data (stars) to results of the best model of high k_r edge turbulence (solid line). The x-axis is the minimum radius of the PCI beam with respect to the separatrix. Achieving a reasonable fit requires non-isotropic turbulence with $L_r < L_\theta$ and $|\bar{k}_r| > |\bar{k}_\theta|$. The region of $\bar{k}_r < 0$ turbulence is located inside the E_r well minimum, and the region of $\bar{k}_r > 0$ turbulence is outside the bottom of the E_r well.

The model is analyzed and the results compared to PCI measurements at $f = 200$ kHz. The inner and outer turbulence layers are referred to respectively with subscripts 1 and 2. When $L_r < L_\theta$, as in H-mode, the location and width of the peaks in the wavenumber spectrum $S(k_{\rm pci}, f = f_0)$ are set by the poloidal parameters, so the experimental data is used directly to determine that $\bar{k}_\theta = 0.8$ cm^{-1} in both regions ($\bar{k}_{\theta,1}\rho_s \sim 0.4$), $L_{\theta,1} = 110 \pm 20$ mm, and $L_{\theta,2} = 160 \pm 10$ mm. Varying $\bar{k}_\theta$ and L_θ from the values determined in this way results in poorer fits. The poloidal parameters are kept fixed and $\bar{k}_{r,1}$, $\bar{k}_{r,2}$, $L_{r,1}$, $L_{r,2}$, $\tilde{n}_1$, and $\tilde{n}_2$ are allowed to vary to minimize the error fitting the experimental data. The best fit and the data used in performing the fits are shown in Fig. 8. The fitting process must be

carefully tuned by hand. The radial profile of the turbulence in the model was chosen for simplicity to have sharp boundaries, so the shapes of the peaks in Fig. 8 are not expected to match the experiment accurately. Error bars on each data point are based on the data scatter in the neighboring points, and an adequate fit requires that these error estimates be chosen carefully. A random search of the space of nine free parameters is not computationally practical, so the turbulence locations are scanned systematically while the plasma parameters are fit to minimize the total weighted squared error between the data points and the modeled curve via stochastic optimization. Convergence of the algorithm requires a good initial guess, but the converged result does not quantitatively depend on the initial guess. In order to be computationally tractable, a rough fit is obtained using the simplified correlation function in Eq. (6), and the result is used as a good initial guess to a new step of optimization using the more accurate Eq. (5). Note that the turbulence model used is the simplest model that can explain the experimental data; removing any one of the free parameters makes even a qualitative match to the data in Fig. 8 impossible. The resulting best fit has parameters $\bar{k}_{r,1} = -1.7 \pm 0.4$ cm^{-1}, $\bar{k}_{r,2} = 9.2 \pm 1.2$ cm^{-1}, $L_{r,2} = 1.0 \pm 0.4$ mm, $\tilde{n}_2/\tilde{n}_1 = 4.2 \pm 0.9$, and $L_{r,1}$ is greater than the width of the turbulence layer and hence unresolved. Note that the correlation length at a single frequency is not the same as the correlation length over the entire frequency range; the values here are restricted to $f = 200$ kHz and the correlation lengths cannot be used to estimate total transport. These parameters satisfy our general expectations, in that $L_r < L_\theta$, $k_{r,1} < 0$ and $k_{r,2} > 0$. Errors are estimated from the model fits. The error on any parameter is the range in the parameter that permits reasonable fits to the data while allowing all other parameters to vary, not the difficulty in determining that parameter with all other parameters remaining fixed. The difference is immense; for example, the relative error in $\tilde{n}_2/\tilde{n}_1$ is $\pm 21\%$ over all sets of parameters that provide equally good matches to the data, but $\tilde{n}_2/\tilde{n}_1$ is determined to within 1% if all other parameters are held constant. The size of the errors reflects not the scatter in the data points but the limitations in the model, especially the simple spatial envelope.

Note the striking result that $|\bar{k}_r| > |\bar{k}_\theta|$. The signal from the outer layer of turbulence is seen to be the dominant contributor to the PCI signal when the beam is nearly tangent to the LCFS. When the PCI beam reaches further into the plasma, $r_{\rm pci} - r_{\rm sep} < -0.04$ m, the PCI signal with $k_{\rm pci} < 0$ records the turbulence inside the E_r well with $\bar{k}_r < 0$, and the PCI signal with $k_{\rm pci} > 0$ reflects the turbulence outside the E_r well with $\bar{k}_r > 0$. Attempts to fit

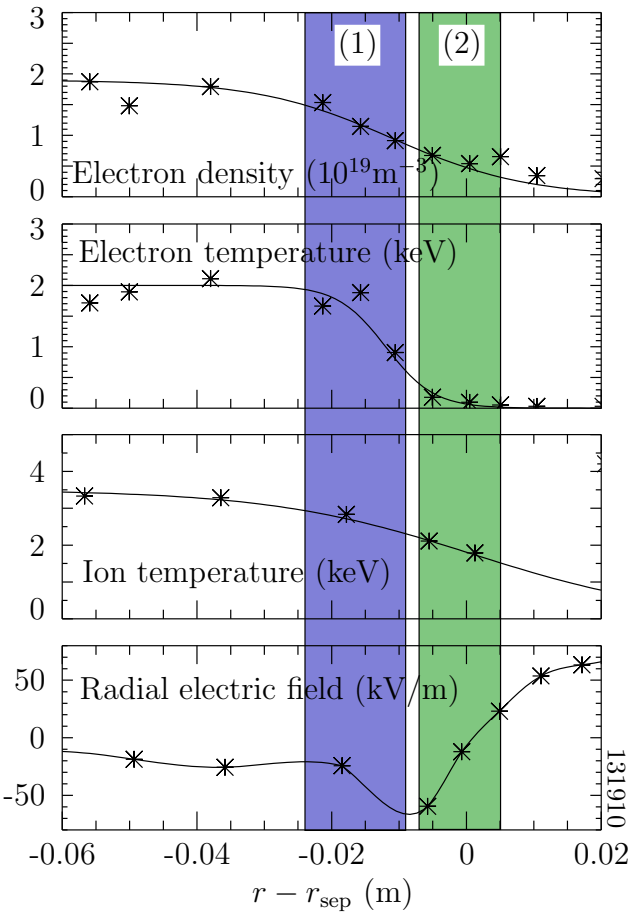

FIG. 9. Profiles of plasma parameters near the separatrix and the locations of layers of turbulence used in modeling PCI results. The dominant radial wavenumber $\bar{k}_r$ is -1.7 cm^{-1} in region 1 and 9.2 cm^{-1} in region 2.

the data with $\bar{k}_r = 0$ were unsuccessful in generating the difference between the PCI signals from above and below the midplane seen in Fig. 6.

The radial extents of the turbulence layers in the model are adjusted to match the experimental data, primarily the width and location of the peak seen in Fig. 6, informed by the results in Sec. III A, and the E_r well structure in Fig. 3. The best fit is found if the outer layer of turbulence fills the region between the 7 mm inside the separatrix (at the midplane) and 5 mm outside the separatrix and the inner region spans the region between flux surfaces at 24 mm and 9 mm inside the separatrix. The locations of the regions of turbulence with respect to the E_r well and pedestal are shown in Fig. 9. Note that the calculated and experimental PCI response is much narrower than the two layers of turbulence, approximately 10 mm vs. 30 mm, due to the effects of line integration. The location in the peak response

in Fig. 6 is consistent with the radial location calculated from the Doppler shift.

The absolute magnitude of the turbulence is determined by cross calibrating with the known amplitude of the EHO. The poloidal structure of the EHO is estimated using a poloidal array of magnetic probes. Similar QH-mode plasmas show peak $\delta n_e = 1.4\times10^{18}$ m^{-3} with a FWHM of 30 mm.[23] The expected PCI signal can then be calculated, including the effect of line integration and the PCI response curve to long wavelength fluctuations, providing an absolute calibration. The absolute magnitude of the turbulence in the model consistent with the PCI data (integrated from 200 kHz to 1 MHz) is $\tilde{n} \sim 2.8 \times 10^{18}$ m^{-3} or $\tilde{n}/n \sim 40\%$ at 3 mm inside the LCFS ($\tilde{n}/n_{\rm ped} \sim 14\%$). The turbulence amplitude is smaller inside the E_r well, $\tilde{n}/n \sim 5\%$ ($\tilde{n}/n_{\rm ped} \sim 3\%$). Note that the turbulence amplitude $\tilde{n}$ is only available from PCI data when complete turbulence parameters can be deduced either from an extensive data set, as is the case here, or from full nonlinear modeling.

IV. DISCUSSION

Plasma physics experiments show a decrease in turbulent transport due to increased shear flow; stabilization of turbulence can be interpreted as the result of distortion of eddies by the shear flow.[10] These tilted, elongated eddies embedded in the flowing plasma give rise in the laboratory frame to the appearance of radial motion; this is equivalent to saying that spectral power in the turbulence is shifted to $k_r \neq 0$. The large shear in the E_r well of QH-mode plasmas is therefore expected to have the side effect of shifting turbulent power to finite k_r. This can be seen by considering a 2d system which includes the Doppler shift from a flow velocity v in the $\hat{y}$ direction with a weak gradient in the x direction $v' = dv/dx$. The shear distorts eddies or other turbulent structures throughout their lifetime τ, equivalent to the autocorrelation time. These lead to the relation for the fluctuations $\tilde{n}(x, y, t) \simeq \tilde{n}(x, y - vt - v'x\tau, 0)$. Applying a Fourier transform and translating into r, θ leads to the relation for the radial wavenumber $\bar{k}_r/\bar{k}_\theta = v'\tau$. This estimate fails if $\bar{k}_\theta = 0$ or $v = 0$. Note that finite value for $\bar{k}_r$ corresponds to radial motion of phase fronts, while all wave power flows purely poloidally. Figure 4 can be used to estimate the autocorrelation time, $\tau \simeq 2/(2\pi\Delta f) = 1.6 \times 10^{-6}$ μs. From Fig. 3, $v' \simeq 1.3 \times 10^6$ s^{-1}, leading to $|\bar{k}_r/\bar{k}_\theta| \simeq 2.2$. The values of $|\bar{k}_r/\bar{k}_\theta|$ deduced from the data are 2.2 and 11.5, similar to or higher than the predicted value, but confirming that large enough velocity shear in the E_r well causes

$|\bar{k}_r| > |\bar{k}_\theta|$. The simple analytic model considered in the previous section does not include physical effects which are expected to change the quantitative results somewhat. Such effects include magnetic shear and radial variation in turbulence amplitude.

The PCI measurements in QH-mode also record a low-frequency mode, seen most strongly at $k_r > 0$ below 100 kHz in Fig. 5(c). Assuming the turbulence generating this signal is within a few centimeters of the separatrix and that the lab-frame frequency results primarily from Doppler shift, we can calculate the poloidal plasma velocity at this location and find its magnitude approximately 25% of that in the high shear region with the same sign. The shape of the edge $V_{\mathbf{E}\times\mathbf{B}}$ (Fig. 3) then implies that the lower frequency component of the PCI signal comes from at least 20 mm inside the separatrix. The EHO complicates further analysis of this component of the signal.

This data was taken in QH-mode because those plasmas maintain constant plasma parameters through the outer gap sweep.[2] The PCI observations however are similar to those seen in ELM-free H-mode without outer gap sweeps, and it is expected that the result of two layers of turbulence with $\bar{k}_r \neq 0$ would be found there if similar measurements could be taken. In contrast, the PCI data taken in L-mode plasmas such as that in Fig. 5(a) shows spectra with no bias towards $k_{\rm pci} > 0$ or $k_{\rm pci} < 0$, suggesting that the turbulence spectrum has a dominant $\bar{k}_r = 0$, as expected when velocity shear is weak.

These results reported here show that the turbulence remains at relatively large amplitude in the E_r well ($\tilde{n}/n \gtrsim 10\%$), even though the turbulence is shifted to $k_r > k_\theta$. This effect is relatively undocumented because low-k turbulence diagnostics cannot generally distinguish between the suppression of turbulence and the shifting of turbulent power to large k_r. While the pressure pedestal in the developed QH-mode edge is well described by the EPED calculation,[7] this high-k_r turbulence may play a role in achieving various high-confinement regimes and in determining energy and particle transport between ELMs (in the absence of the EHO), which are issues of vital importance to future machines.

V. ACKNOWLEDGEMENTS

This work was supported in part by the US Department of Energy under DE-FG02-94ER54235 and DE-FC02-04ER54698.

REFERENCES

[1]J. L. Luxon, Nucl. Fusion **42**, 614 (2002).

[2]K. H. Burrell, W. P. West, E. J. Doyle, M. E. Austin, T. A. Casper, P. Gohil, C. M. Greenfield, R. J. Groebner, A. W. Hyatt, R. J. Jayakumar, D. H. Kaplan, L. L. Lao, A. W. Leonard, M. A. Makowski, G. R. McKee, T. H. Osborne, P. B. Snyder, W. M. Solomon, D. M. Thomas, T. L. Rhodes, E. J. Strait, M. R. Wade, G. Wang, and L. Zeng, Phys. Plasmas **12**, 056121 (2005).

[3]K. H. Burrell, M. E. Austin, D. P. Brennan, J. C. DeBoo, E. J. Doyle, C. Fenzi, C. Fuchs, P. Gohil, C. M. Greenfield, R. J. Groebner, L. L. Lao, T. C. Luce, M. A. Makowski, G. R. McKee, R. A. Moyer, C. C. Petty, M. Porkolab, C. L. Rettig, T. L. Rhodes, J. C. Rost, B. W. Stallard, E. J. Strait, E. J. Synakowski, M. R. Wade, J. G. Watkins, and W. P. West, Phys. Plasmas **8**, 2153 (2001).

[4]K. H. Burrell, T. H. Osborne, P. B. Snyder, W. P. West, M. E. Fenstermacher, R. J. Groebner, P. Gohil, A. W. Leonard, and W. M. Solomon, Nucl. Fusion **49**, 085024 (2009).

[5]A. M. Garofalo, W. M. Solomon, J.-K. Park, K. H. Burrell, J. C. DeBoo, M. J. Lanctot, G. R. McKee, H. Reimerdes, L. Schmitz, M. J. Schaffer, and P. B. Snyder, Nucl. Fusion **51**, 083018 (2011).

[6]C. Holland, L. Schmitz, T. L. Rhodes, W. A. Peebles, J. C. Hillesheim, G. Wang, L. Zeng, E. J. Doyle, S. P. Smith, R. Prater, K. H. Burrell, J. Candy, R. E. Waltz, J. E. Kinsey, G. M. Staebler, J. C. DeBoo, C. C. Petty, G. R. McKee, Z. Yan, and A. E. White, Phys. Plasmas **18**, 056113 (2011).

[7]P. B. Snyder, T. H. Osborne, K. H. Burrell, R. J. Groebner, A. W. Leonard, R. Nazikian, D. M. Orlov, O. Schmitz, M. R. Wade, and H. R. Wilson, Phys. Plasmas **19**, 056115 (2012).

[8]C. F. Maggi, Nucl. Fusion **50**, 066001 (2010).

[9]H. Biglari, P. H. Diamond, and P. W. Terry, Phys. Fluids B **2**, 1 (1990).

[10]P. W. Terry, Rev. Mod. Phys. **72**, 109 (2000).

[11]L. Lin, M. Porkolab, E. M. Edlund, J. C. Rost, M. Greenwald, N. Tsujii, J. Candy, R. E. Waltz, and D. R. Mikkelsen, Plasma Phys. Control. Fusion **51**, 065006 (2009).

[12]L. Lin, M. Porkolab, E. M. Edlund, J. C. Rost, C. L. Fiore, M. Greenwald, Y. Lin, D. R. Mikkelsen, N. Tsujii, and S. J. Wukitch, Phys. Plasmas **16**, 012502 (2009).

[13]M. Porkolab, J. Dorris, P. Ennever, C. Fiore, M. Greenwald, A. Hubbard, Y. Ma, E. Marmar, Y. Podpaly, M. L. Reinke, J. E. Rice, J. C. Rost, N. Tsujii, D. Ernst, J. Candy, G. M. Staebler, and R. E. Waltz, Plasma Phys. Control. Fusion **54**, 124029 (2012).

[14]H. Weisen, Plasma Phys. Control. Fusion **28**, 1147 (1986).

[15]S. C. Coda, M. Porkolab, and K. H. Burrell, Phys. Letters A **273**, 125 (2000).

[16]S. Coda, M. Porkolab, and K. H. Burrell, Phys. Rev. Lett. **86**, 4835 (2001).

[17]S. Coda, M. Porkolab, and K. H. Burrell, Nucl. Fusion **41**, 1885 (2001).

[18]S. Coda, M. Porkolab, and T. N. Carlstrom, Rev. Sci. Instrum. **63**, 4974 (1992).

[19]J. R. Dorris, J. C. Rost, and M. Porkolab, Rev. Sci. Instrum. **80**, 023503 (2009).

[20]T. N. Carlstrom, G. L. Campbell, J. C. DeBoo, R. Evanko, J. Evans, C. M. Greenfield, J. Haskovec, C. L. Hsieh, E. McKee, R. T. Snider, R. Stockdale, P. K. Trost, and M. P. Thomas, Rev. Sci. Instrum. **63**, 4901 (1992).

[21]K. H. Burrell, D. H. Kaplan, P. Gohil, D. G. Nilson, R. J. Groebner, and D. M. Thomas, Rev. Sci. Instrum. **72**, 1028 (2001).

[22]K. H. Burrell, W. P. West, E. J. Doyle, M. E. Austin, J. S. deGrassie, P. Gohil, C. M. Greenfield, R. J. Groebner, R. Jayakumar, D. H. Kaplan, L. L. Lao, A. W. Leonard, M. A. Makowski, G. R. McKee, W. M. Solomon, D. M. Thomas, T. L. Rhodes, M. R. Wade, G. Wang, J. G. Watkins, and L. Zeng, Plasma Phys. Control. Fusion **46**, A165 (2004).

[23]L. Zeng, G. Wang, E. J. Doyle, T. L. Rhodes, W. A. Peebles, G. R. McKee, R. Fonck, K. H. Burrell, M. E. Fenstermacher, J. Boedo, and R. Moyer, Plasma Phys. Control. Fusion **46**, A121 (2004).